Supplementary Information

Hierarchical self-assembly induced supramolecular polymer helical nanowires with white circularly polarized luminescence

Shuai Qiu, Zhao Gao,* Xin Song, Xiao Hu, Hongxing Yuan, and Wei Tian*

*MOE Key Laboratory Materials Physics and Chemistry in Extraordinary Condition, Shaanxi Key Laboratory of Macromolecular Science and Technology, School of Science, Northwestern Polytechnical University, Xi'an, 710072, P. R. China

1. Materials and methods

4-Hydroxybenzaldehyde, 1-chloro-6-hydroxyhexane, potassium iodide, potassium carbonate, 2-acetylpyridine, ammonium hydroxide, and imidazole were purchased from Aladdin Reagents, China. Bis(triphenylphosphine)palladium(II) chloride, tris(4-bromophenyl)amine, bis(pinacolato)diboron, and 4-bromobenzaldehydewere purchased from TCI, Japan. 4-dimethylaminopyridine (DMAP) was purchased from J&K Scientific Ltd, China. N,N'-Dicyclohexylcarbodiimide, europium(iii) trifluoromethanesulfonate, 3,4,9,10-perylenetetracarboxylic dianhydride, and zinc acetate dihydrate were purchased from Adamas, China. Sodium hydroxide, potassium iodide was purchased from Macklin, China. Other chemical reagents were purchased from Inno-Chem, China. Inorganic salts and organic solvents were purchased from Tianjin Kermel Chemical Reagents Development Center. Organic solvents were dried with 4 Å grade molecular sieves before use. All agents were used as received unless special statement.

^{1}H NMR and ^{13}C NMR spectra in solution were obtained from Bruker Avance 400 instruments. Multiplicities are denoted as follows: s = singlet, d = doublet, and m = multiplet. 2D diffusion-ordered NMR (DOSY) experiments were performed on a Bruker AVANCE III 600 MHz spectrometer. Ultraviolet visible (UV–Vis) spectra were recorded on a Shimadzu UV-2550 spectrometer. Cuvette geometry used in these experiments is length*width*height = 12.5*12.5*45 mm, optical path: 3 mm. Fluorescence spectra were recorded with a Hitachi F-4600 FL Spectrophotometer. For fluorescence measurements, slit width = 5 nm, voltage = 500 V. The time-resolved fluorescence lifetime experiments were performed with an Edinburgh FLS980 transient steady-state fluorescence spectrometer. Quantum yields were measured by using an integrating sphere on a HAMAMATSU Quantaurus-QY C11347-11. High-resolution electrospray ionization mass spectra (HR-ESI-MS) were obtained on a Bruker Esquire 3000 plus mass spectrometer equipped with an ESI interface and ion trap analyzer. Atomic force microscopy (AFM) images were obtained on a Bruker Dimension FastScan and Dimension Icon instrument. Transmission electron microscope (TEM) experiments were performed on a FEI Talos F200X TEM instrument. Scanning electron microscopy (SEM) investigations were conducted on a FEI Verios G4 instrument. The sample preparation procedures for the microscopies are as follows: the toluene solution of each sample was first dropped onto the corresponding substrates, and then the toluene solvent was slowly evaporated at room temperature. Circular dichroism (CD) spectra were acquired using the JASCO J815 spectrophotometer. Circularly polarized luminescence (CPL) spectra were acquired using the JASCO CPL-200 spectrofluoropolarimeter. Dynamic light scattering (DLS) measurements

were carried out on a Brookhaven BI-9000AT system (Brookhaven Instruments Corporation, USA), using a 200-mW polarized laser source (λ = 630 nm). The critical aggregation concentration (CAC) values were determined on a DDS-307 instrument. Fourier transform infrared spectra (FT-IR) were recorded on a Jasco FTIR-660 spectrometer. Dissipative particle dynamics (DPD) simulations. DPD simulations [S1] were carried out using the Mesocite module in Materials Studio to investigate the self-assembly process of supramolecular coordination polymers (SCPs) derived from *D*-M_1, M_2 and Eu^{3+} ions. Four different components were modeled in the system: *D*-M_1, M_2, Eu^{3+} ions, and toluene solvent. The repulsion parameters between DPD beads were calculated from Flory-Huggins parameters as reported previously.[S2] In the DPD method, the force F_{ij} exerted on bead *i* by bead *j* consists of a conservative force F_{ij}^C, a dissipative force F_{ij}^D, and a radon force F_{ij}^R. Thus, the total force f_i is given by

$$f_i = \sum_{j \neq i} \left(F_{ij}^C + F_{ij}^D + F_{ij}^R \right) + f_i^s + f_i^A$$

The remaining terms are forces due to bonded interactions: springs (*S*) and angles (*A*). To determine the repulsive interaction parameters, Groot and Warren established the relationship between the χ-parameter in Flory-Huggins theory and a_{ij}as follows:

$$a_{ij} = a_{ii} + 3.27\chi_{ij}$$

where a_{ii} = 25 for the same type of bead. In this article, the χ-parameters between different species were estimated from the Blends module by using the COMPASS force field.[S3] In this study, M_1 and M_2 with a ratio of 1 : 1 were placed in a cubic simulation box of 150 × 150 × 150 $Å^3$ and periodic boundary conditions were applied. The density of the whole system is 3 in reduced units.

2. Synthetic routes to monomers M_1 and M_2.

The desired monomers *D*-M_1 and M_2 have been shown in Scheme S1. PDI-based monomer *D*-M_1 contains two-sets of symmetrical lysine and polypyridine, linking on the periphery of PDI unit via ester bonds (Scheme S1). In *D*-M_1, PDI is used as the fluorophore and *D*-lysine is the chiral source. The two groups also provide the non-covalent driving forces (π–π staking and hydrogen bonding interactions) for the hierarchical self-assembly. M_2 takes three-sets of symmetrical terpyridine, covalent linking with triphenylamine through Suzuki coupling reaction (Scheme S2). Rigid monomer M_2 is conducive to avoiding the chiral-silent phenomenon occurrence, ascribing to the chain entanglements during the self-assembly process. Detailed synthetic procedures and characterization results of two monomers are shown as follows.

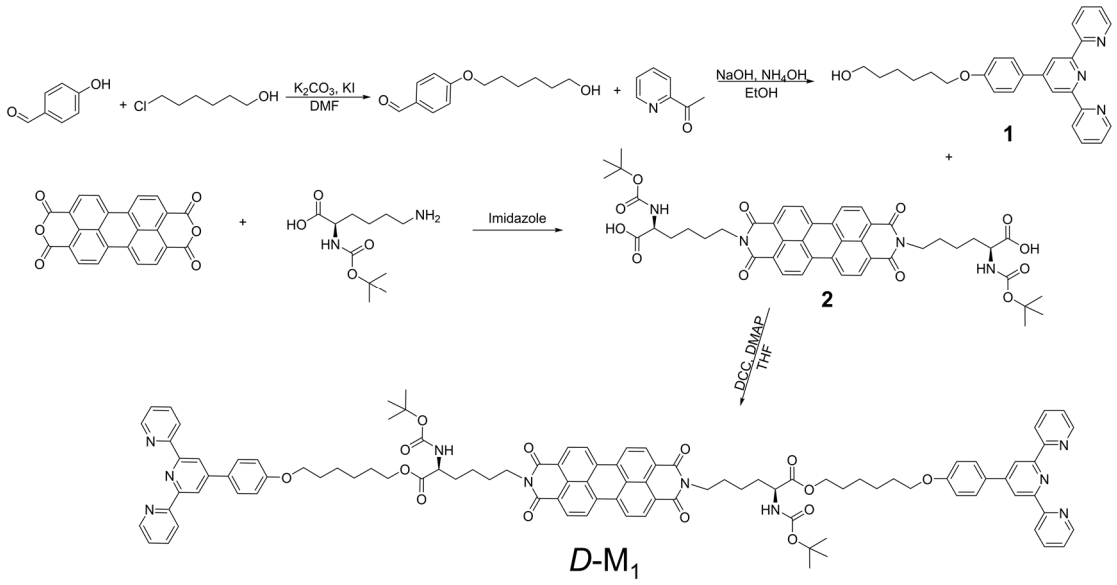

Scheme S1. Synthetic routes to monomer *D*-M_1.

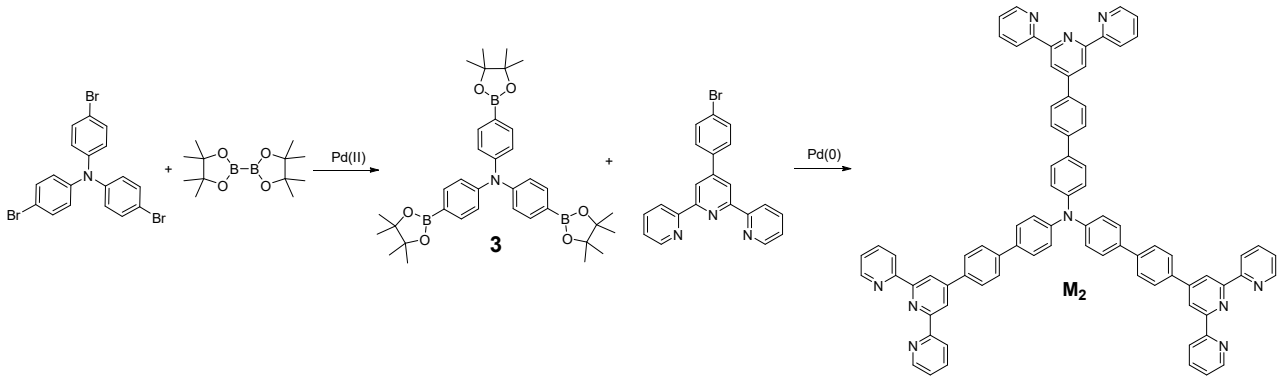

Scheme S2. Synthetic routes to monomer M_2.

2.1 Synthesis of 6-(4-([2,2':6',2''-terpyridin]-4'-yl)phenoxy)hexan-1-ol (1).

The synthesis of intermediate 6-(4-([2,2':6',2''-terpyridin]-4'-yl)phenoxy)hexan-1-ol were referred to our previous synthesis.[S4] ^{1}H NMR (400 MHz, $CDCl_3$) δ (ppm) 8.71 (d, J = 4.3, 1H), 8.69 (s, 1H), 8.65 (d, J = 7.9, 1H), 7.89 – 7.81 (m, 2H), 7.33 (dd, J = 6.7, 5.0, 1H), 7.00 (d, J = 8.7, 1H), 3.99 (t, J = 6.5, 2H), 3.65 (t, J = 6.5, 1H), 1.79 (dd, J = 14.4, 6.7, 1H), 1.60 (dd, J = 14.1, 7.0, 1H), 1.53 – 1.45 (m, 1H), 1.42 (dd, J = 10.1, 5.5, 1H).

2.2 Synthesis of (2S,2'S)-6,6'-(1,3,8,10-tetraoxo-1,3,8,10-tetrahydroanthra[2,1,9-def:6,5,10-d'e'f']diisoquinoline-2,9-diyl)bis(2-((tert butoxycarbonyl)amino)hexanoic acid) (2).

3,4,9,10-Perylenetetracarboxylic dianhydride (1.96 g, 5 mmol, 1.0 eq.), imidazole (10.0 g) and a catalytic amount of zinc acetate (50 mg, 0.1 eq.) were heated to 105 °C with stirring under N_2 atmosphere. Upon melting of the imidazole, (tert-butoxycarbonyl)-D-lysine (6.15 g, 25 mmol, 5.0 eq.) was added and the mixture was left to stir for 16 h. The crude product was treated with MeOH (60 mL) and 2.0 M HCl solution (20 mL), and then the mixture was filtered. The residue was washed with MeOH (2 × 50 mL) and Et_2O (2 × 50 mL) and dried under vacuum, fuchsia solids were obtained with 64% yield. ^{1}H NMR (400 MHz, DMSO) δ (ppm) 12.20–12.70 (s, 2H), 7.60–7.81 (m, 6H), 7.04 (d, J = 7.5 Hz, 2H), 4.12–3.68 (m, 6H), 3.24–3.38 (m, 4H), 1.47–1.78 (m, 8H), 1.38 (s, 18H). ^{13}C NMR (100 MHz, DMSO) δ (ppm) 174.37, 161.63, 155.66, 131.84, 129.15, 126.53, 122.75, 120.83, 77.97, 53.57, 30.64, 28.13, 28.00, 27.50, 23.35.

2.3 Synthesis of monomer *D*-M_1.

(2S,2'S)-6,6'-(1,3,8,10-Tetraoxo-1,3,8,10-tetrahydroanthra[2,1,9-def:6,5,10-d'e'f']diisoquinoline-2,9-diyl)bis(2-((tert-butoxycarbonyl)amino)hexanoic acid) (848 mg, 1.0 mmol, 1.0 eq.), N,N'-dicyclohexylcarbodiimide (DCC) (309 mg, 1.5 mmol, 1.5 eq.), DMAP (122 mg, 1.0 mmol, 1.0 eq.) were dissolved in tetrahydrofuran solution under ice bath for 15 minutes, 6-(4-([2,2':6',2''-terpyridin]-4'-yl)phenoxy)hexan-1-ol (935 mg, 2.2 mmol, 2.2 eq.) was added and the mixture was left to stir for 16 h. 50 ml water was added to the reaction solution and extracted with CH_2Cl_2 (3 × 50 mL). The extracts were dried over anhydrous sodium sulfate, and purified by column chromatography (petroleum ether/dichloromethane, 10 : 1 v/v as the eluent) to give *D*-M_1 as fuchsia solids (1.15 g, 71%). ^{1}H NMR (400 MHz, $CDCl_3$) δ (ppm) 8.65 (d, J = 4.1 Hz, 4H), 8.44 (d, J = 7.9 Hz, 4H), 8.37 (d, J = 8.0 Hz, 8H), 8.16 (d, J = 7.9 Hz, 4H), 7.80 (t, J = 7.5 Hz, 4H), 7.60 (d, J = 8.4 Hz, 4H), 7.36–7.30 (m, 4H), 6.87 (d, J = 8.5 Hz, 4H), 5.20 (d, J = 7.9 Hz, 4H), 4.35 (m, 6H), 4.23–4.17 (m, 2H), 4.17–4.10 (m, 4H), 4.02 (t, J = 6.3 Hz, 4H), 2.11–1.71 (m, 20H), 1.57 (d, J = 5.1 Hz, 4H), 1.48 (s, 18H). ^{13}C NMR (100 MHz,

$CDCl_3$) δ (ppm) 172.99, 162.96, 159.96, 155.84, 155.48, 155.15, 148.92, 148.45, 136.62, 133.80, 130.68, 129.34, 128.52, 127.85, 125.48, 123.69, 122.57, 120.95, 117.12, 114.56, 79.80, 67.78, 65.34, 53.56, 40.00, 32.39, 31.63, 29.26, 28.47, 27.64, 26.01, 25.64, 22.96. HRMS (ESI-TOF) ($C_{100}H_{98}N_{10}O_{14}$): m/z calcd for $[M+H]^+$ = 1662.7264, found = 1663.3204.

2.4 Synthesis of monomer *L*-M_1.

The preparation procedure of *L*-M_1 is similar to *D*-M_1. The yield of *L*-M_1 is 73%. ^{1}H NMR (400 MHz, $CDCl_3$) δ (ppm) 8.65 (d, J = 4.1 Hz, 4H), 8.44 (d, J = 7.9 Hz, 4H), 8.37 (d, J = 8.0 Hz, 8H), 8.16 (d, J = 7.9 Hz, 4H), 7.80 (t, J = 7.5 Hz, 4H), 7.60 (d, J = 8.4 Hz, 4H), 7.36–7.30 (m, 4H), 6.87 (d, J = 8.5 Hz, 4H), 5.19 (d, J = 7.9 Hz, 4H), 4.35 (m, 6H), 4.22–4.18 (m, 2H), 4.17–4.10 (m, 4H), 4.02 (t, J = 6.3 Hz, 4H), 2.11–1.71 (m, 20H), 1.57 (d, J = 5.1 Hz, 4H), 1.48 (s, 18H). ^{13}C NMR (100 MHz, $CDCl_3$) δ (ppm) 172.99, 162.96, 159.96, 155.84, 155.48, 155.15, 148.92, 148.45, 136.62, 133.80, 130.68, 129.34, 128.52, 127.85, 125.48, 123.69, 122.57, 120.95, 117.12, 114.56, 79.80, 67.79, 65.33, 53.57, 40.00, 32.38, 31.63, 29.26, 28.47, 27.64, 26.01, 25.64, 22.96. HRMS (MALDI-TOF) ($C_{100}H_{98}N_{10}O_{14}$): m/z calcd for $[M+H]^+$ = 1662.7264, found = 1663.7330.

2.5 Synthesis of tris(4-(4,4,5,5-tetramethyl-1,3,2-dioxaborolan-2-yl)phenyl)amine (3).

Tris(4-bromophenyl)amine (1.446 g, 3.0 mmol, 1.0 eq.), bis(pinacolato)diboron (1.524 g, 6.0 mmol, 2.0 eq.), and zinc acetate dihydrate (1.971 g, 9.0 mmol, 3 eq.) were added into a Schlenck tube and degassed with N_2. The dispersion of $Pd(PPh_3)_2Cl_2$ (210 mg, 0.3 mmol, 0.1 eq.) in DMSO (50 mL) were degassed using N_2 and then injected into the Schlenck tube. After stirring in the dark at 110 ℃ for 72 hours, the reaction mixture was poured into ice water, and the residue was extracted with CH_2Cl_2 for three times. The combined organic layer was dried over anhydrous $MgSO_4$, and the solvent was removed with a rotary evaporator. The residue was purified by flash column chromatography (CH_2Cl_2/THF, 15 : 1 v/v as the eluent) to afford compound tris(4-(4,4,5,5-tetramethyl-1,3,2-dioxaborolan-2-yl)phenyl)amine as white solids (1.14 g, 61%). ^{1}H NMR (400 MHz, $CDCl_3$) δ (ppm) 7.68 (d, J = 8.3 Hz, 6H), 7.07 (d, J = 8.3 Hz, 6H), 1.33 (s, 36H). ^{13}C NMR (100 MHz, $CDCl_3$) δ (ppm) 149.88, 136.04, 123.59, 83.79, 24.99.

2.6 Synthesis of monomers M_2.

Tris(4-(4,4,5,5-tetramethyl-1,3,2-dioxaborolan-2-yl)phenyl)amine (608 mg, 1.0 mmol, 1.0 eq.) and 4'-(4-bromophenyl)-2,2':6',2''-terpyridine (1.277 g, 3.3 mmol, 3.3 eq.) were added into a

Schlenck tube and degassed with N_2. K_2CO_3 aqueous solution (4 M, 20 mL) and THF (50 mL) were degassed using N_2 and then injected into the Schlenck tube. After stirring in the dark at 70 ℃ for 48 hours, the reaction mixture was evaporated to remove the solvent, and the residue was extracted with 50 mL of CH_2Cl_2 for three times. The combined organic layer was dried over anhydrous $MgSO_4$, and the solvent was removed with a rotary evaporator. The residue was purified by flash column chromatography (CH_2Cl_2/THF, 15 : 1 v/v as the eluent) to afford monomer M_2 as yellow solid (606 mg, 52 %). ^{1}H NMR (400 MHz, $CDCl_3$) δ (ppm) 8.84 (s, 6H), 8.78 (d, J = 4.0 Hz, 6H), 8.72 (d, J = 7.9 Hz, 6H), 8.05 (d, J = 8.4 Hz, 6H), 7.93 (td, J = 7.8, 1.8 Hz, 6H), 7.80 (d, J = 8.4 Hz, 6H), 7.67 (d, J = 8.6 Hz, 6H), 7.42 – 7.38 (m, 6H), 7.35 (d, J = 8.6 Hz, 6H). ^{13}C NMR (100 MHz, $CDCl_3$) δ (ppm) 156.68, 156.26, 149.91, 149.29, 147.17, 141.32, 137.00, 136.95, 135.03, 128.01, 127.55, 127.26, 124.69, 123.98, 121.53, 118.78. HRMS (ESI-TOF) ($C_{81}H_{54}N_{10}$): m/z calcd for $[M+H]^+$ = 1166.4533, found = 1166.5278.

3. Supplementary Figures

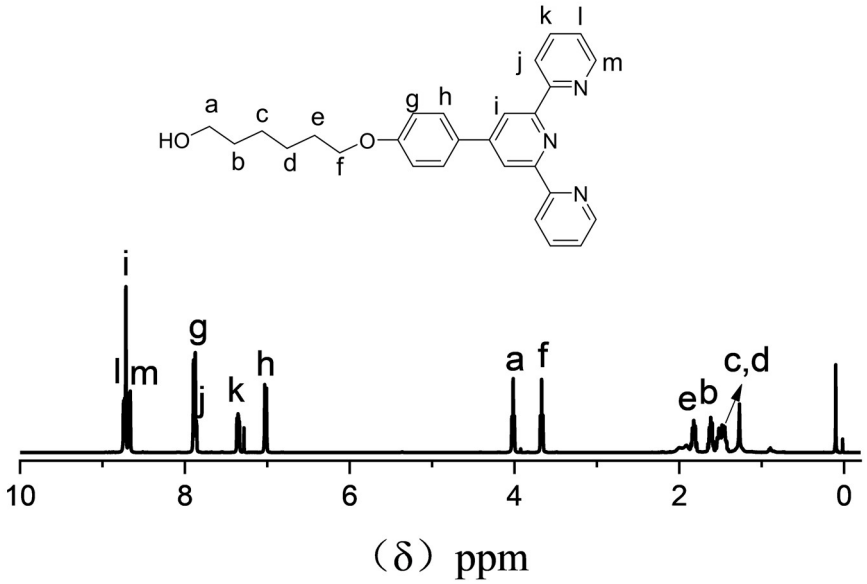

Figure S1. ^{1}H NMR spectrum (400 MHz, $CDCl_3$, room temperature) of 6-(4-([2,2':6',2''-terpyridin]-4'-yl)phenoxy)hexan-1-ol (1).

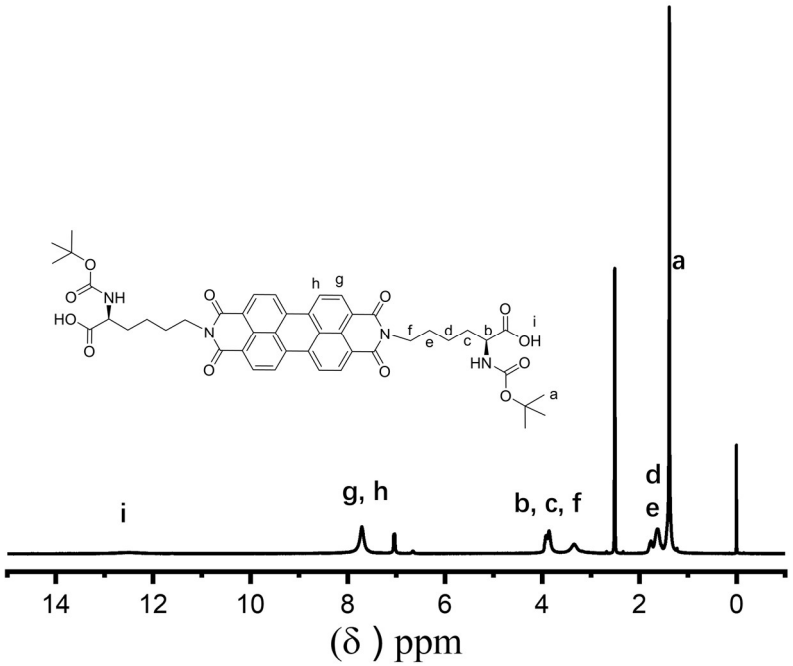

Figure S2. ^{1}H NMR spectrum (400 MHz, DMSO-d_6, room temperature) of (2S,2'S)-6,6'-(1,3,8,10-tetraoxo-1,3,8,10-tetrahydroanthra[2,1,9-def:6,5,10-d'e'f']diisoquinoline-2,9-diyl)bis(2-((tert-butoxycarbonyl)amino)hexanoic acid) (2).

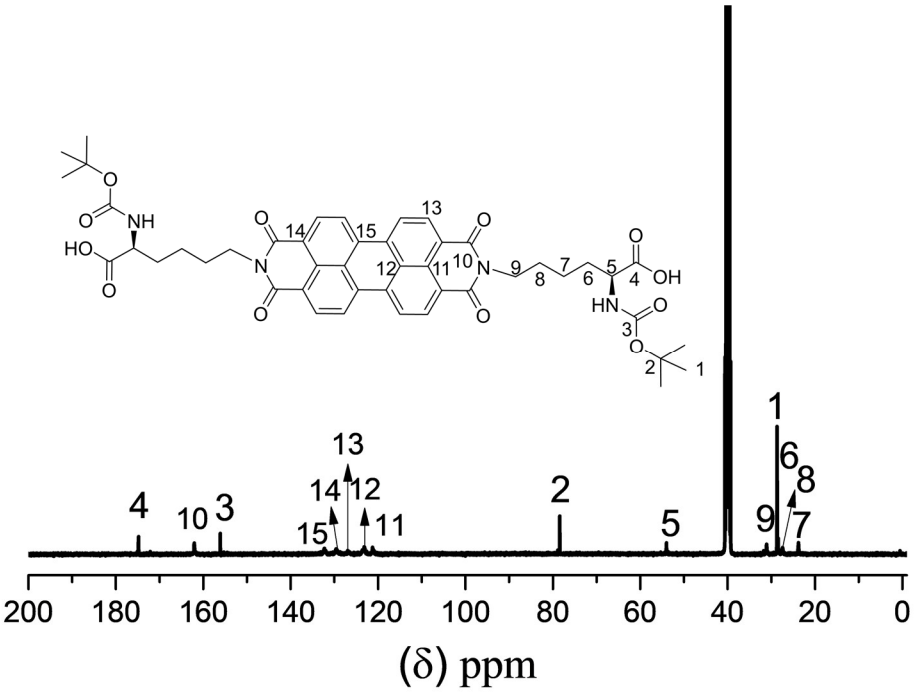

Figure S3. ^{13}C NMR spectrum (100 MHz, DMSO-d_6, room temperature) of (2S,2'S)-6,6'-(1,3,8,10-tetraoxo-1,3,8,10-tetrahydroanthra[2,1,9-def:6,5,10-d'e'f']diisoquinoline-2,9-diyl)bis(2-((tert-butoxycarbonyl)amino)hexanoic acid) (2).

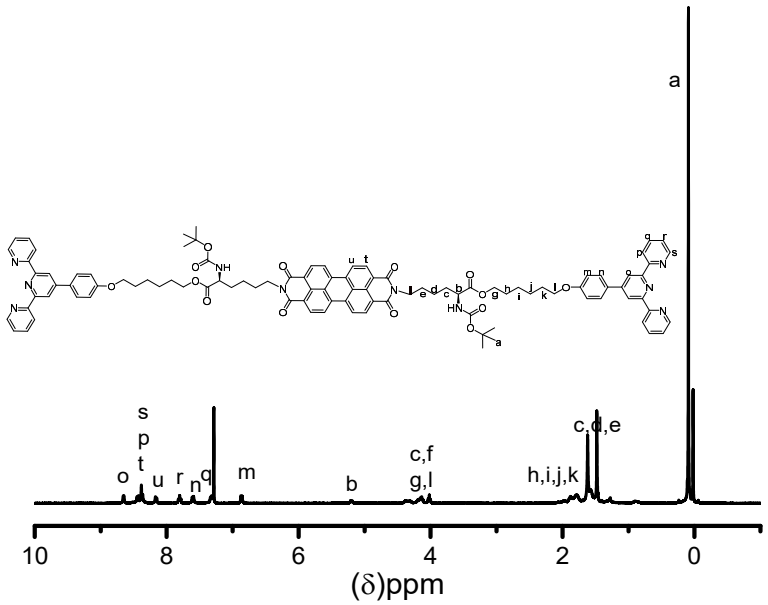

Figure S4. ^{1}H NMR spectrum (400 MHz, $CDCl_3$, room temperature) of monomer *D*-M_1.

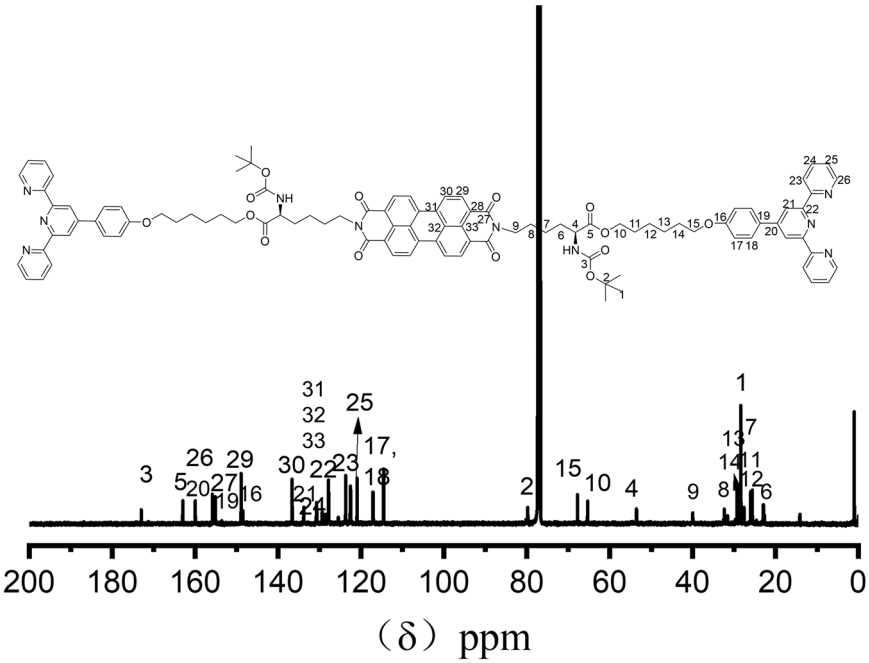

Figure S5. ^{13}C NMR spectrum (100 MHz, $CDCl_3$, room temperature) of monomer *D*-M_1.

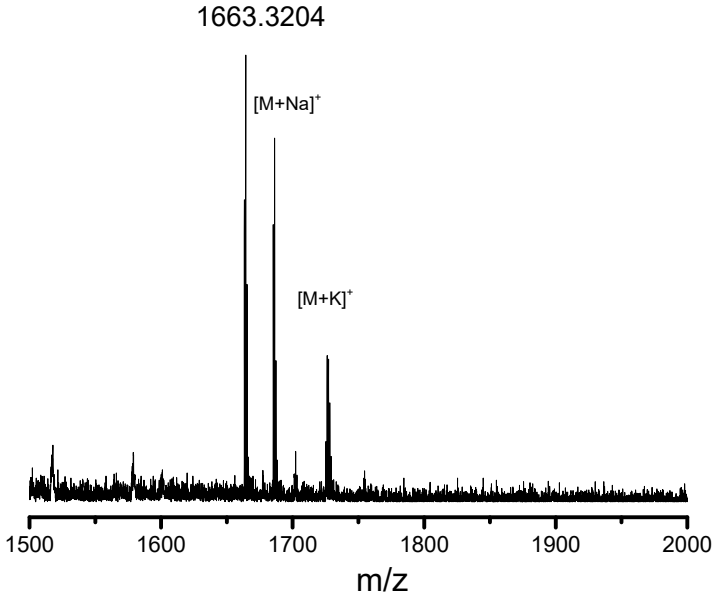

Figure S6. High-resolution electrospray ionization mass spectra of monomer *D*-M_1.

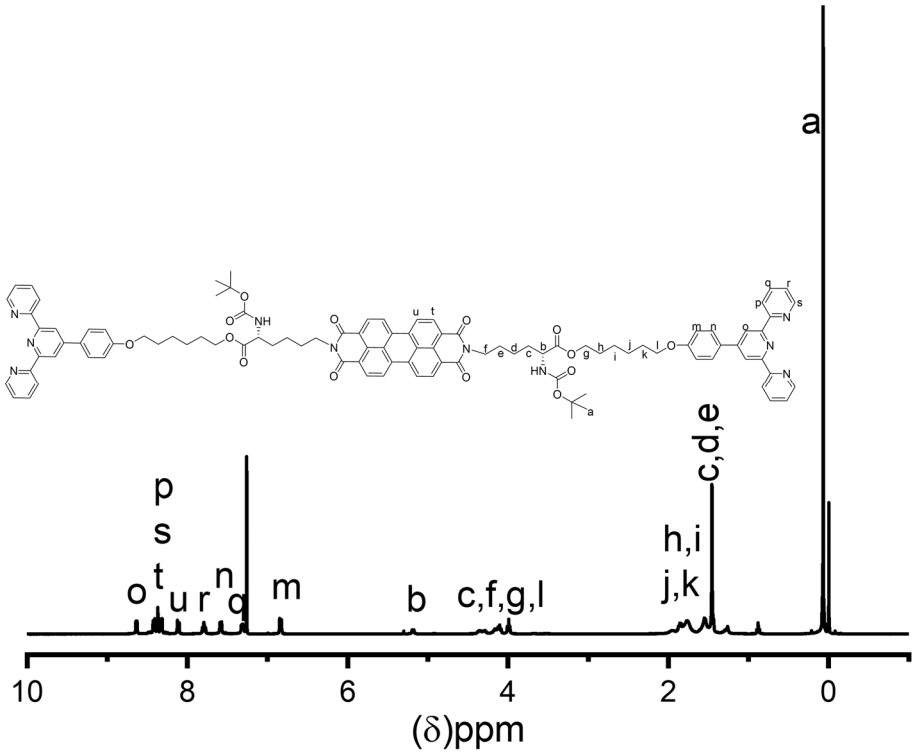

Figure S7. ^{1}H NMR spectrum (400 MHz, $CDCl_3$, room temperature) of monomer *L*-M_1.

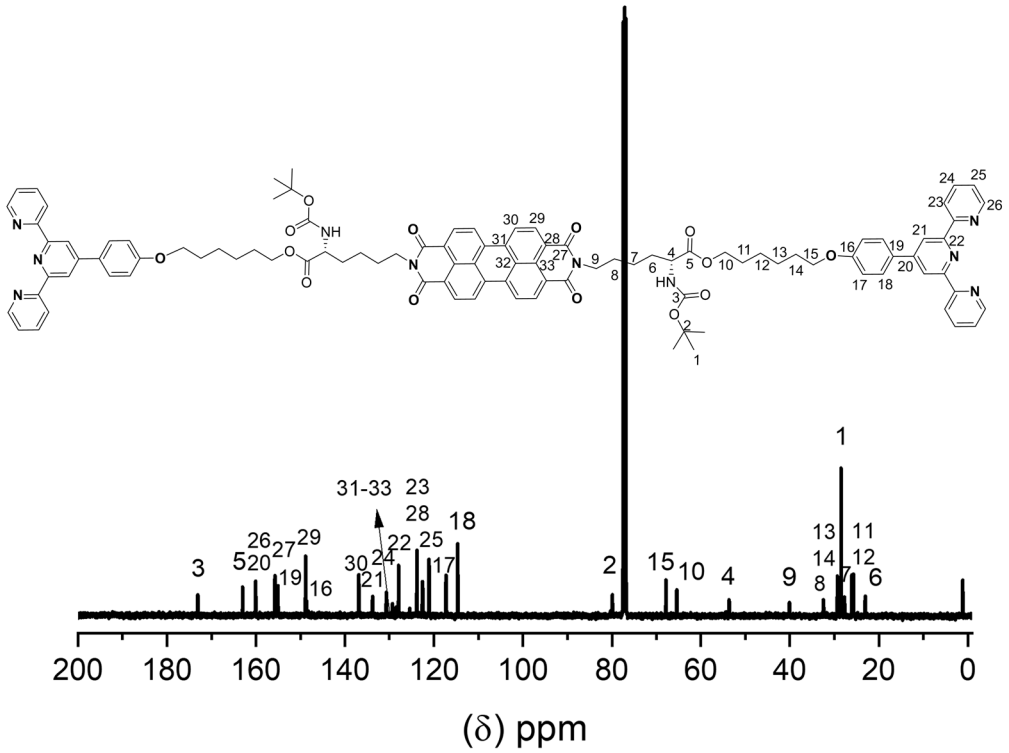

Figure S8. ^{13}C NMR spectrum (100 MHz, $CDCl_3$, room temperature) of monomer *L*-M_1.

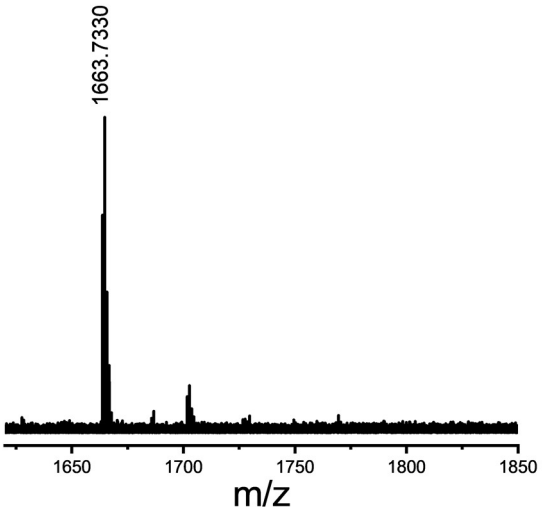

Figure S9. High-resolution electrospray ionization mass spectra of monomer *L*-M_1.

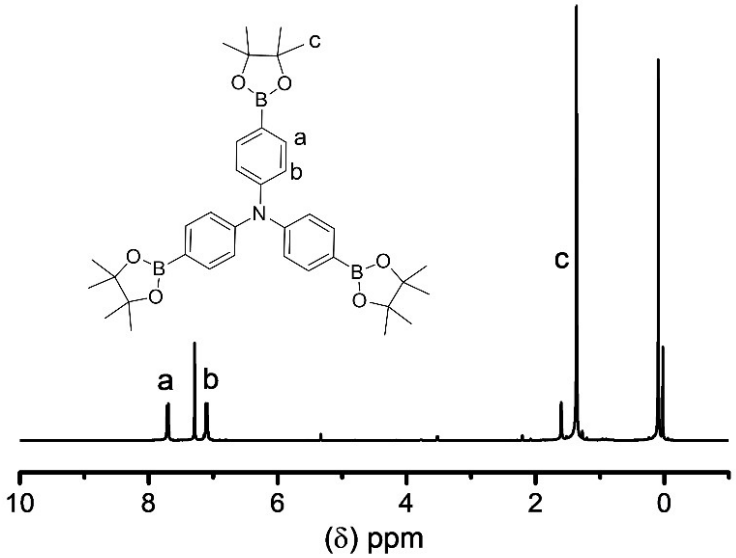

Figure S10. ^{1}H NMR spectrum (400 MHz, $CDCl_3$, room temperature) of tris(4-(4,4,5,5-tetramethyl-1,3,2-dioxaborolan-2-yl)phenyl)amine (3).

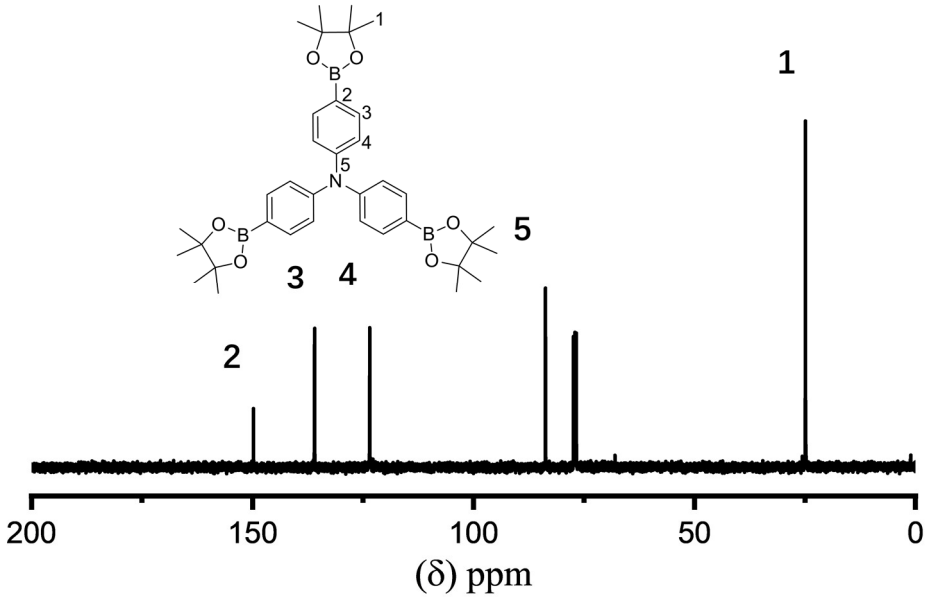

Figure S11. ^{1}H NMR spectrum (100 MHz, $CDCl_3$, room temperature) of tris(4-(4,4,5,5-tetramethyl-1,3,2-dioxaborolan-2-yl)phenyl)amine (3).

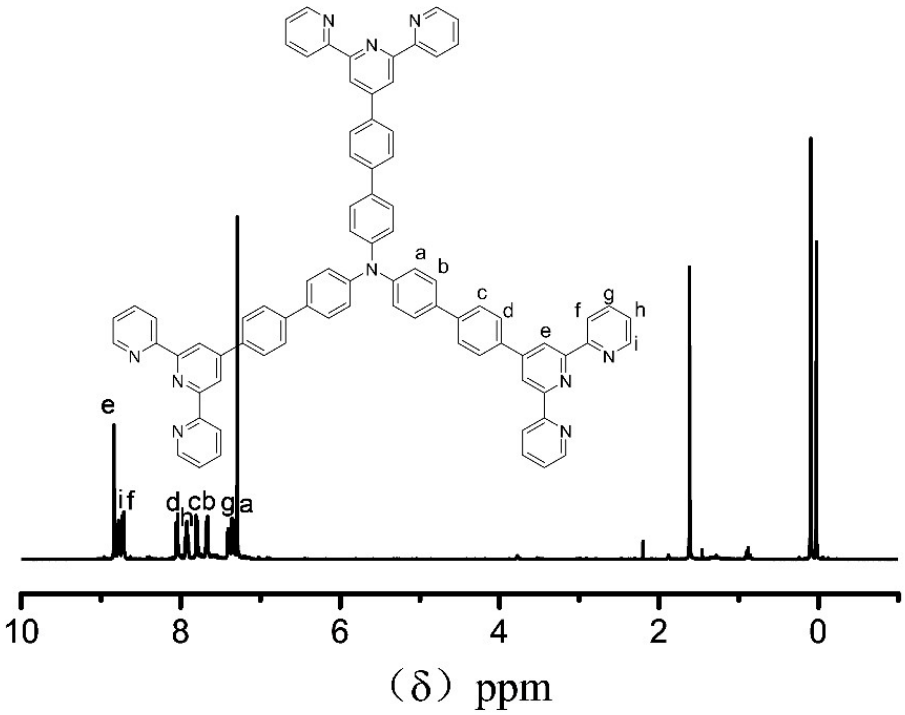

Figure S12. ^{1}H NMR spectrum (400 MHz, $CDCl_3$, room temperature) of monomer M_2.

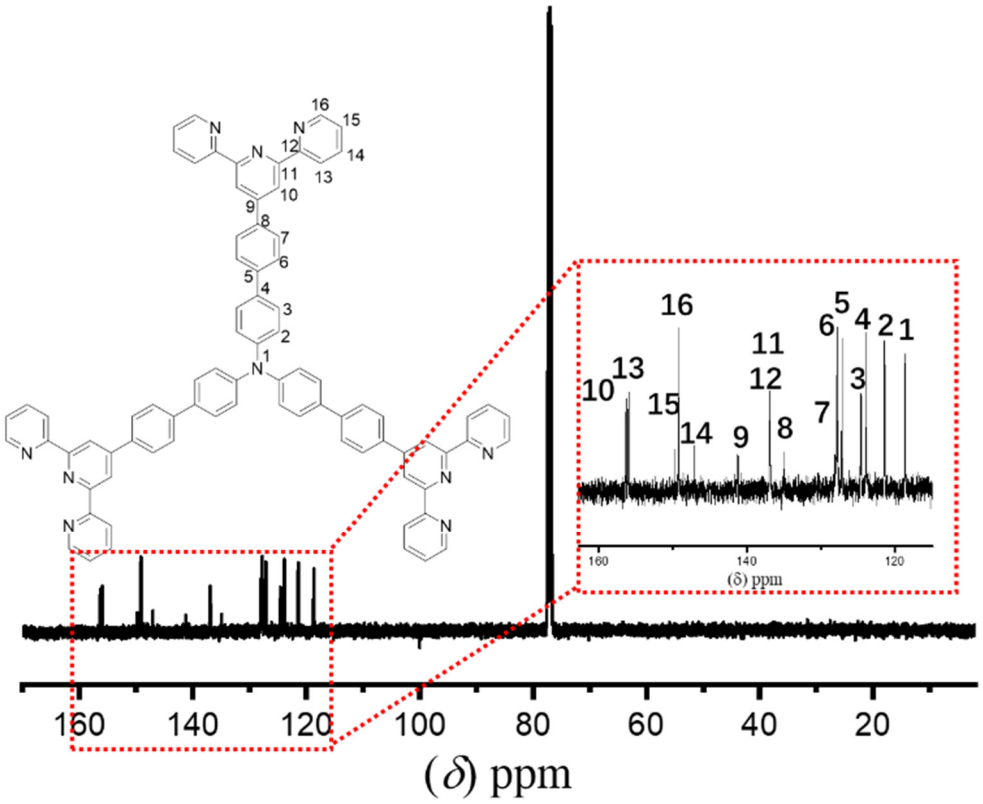

Figure S13. ^{1}H NMR spectrum (100 MHz, $CDCl_3$, room temperature) of monomer M_2.

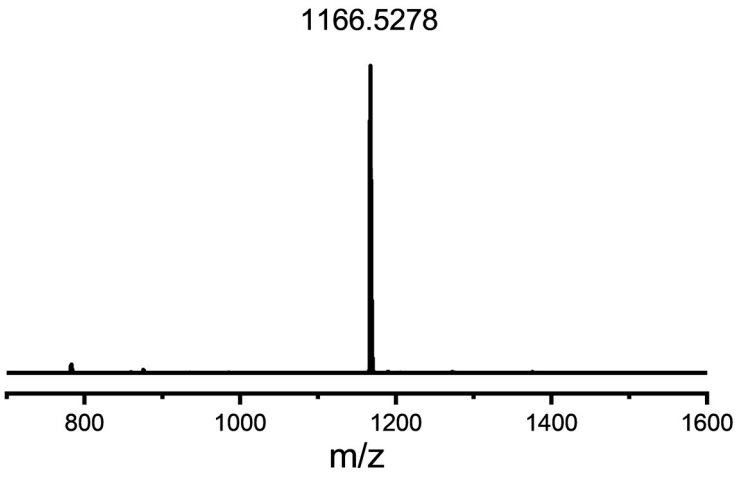

Figure S14. High-resolution electrospray ionization mass spectra of monomer M_2.

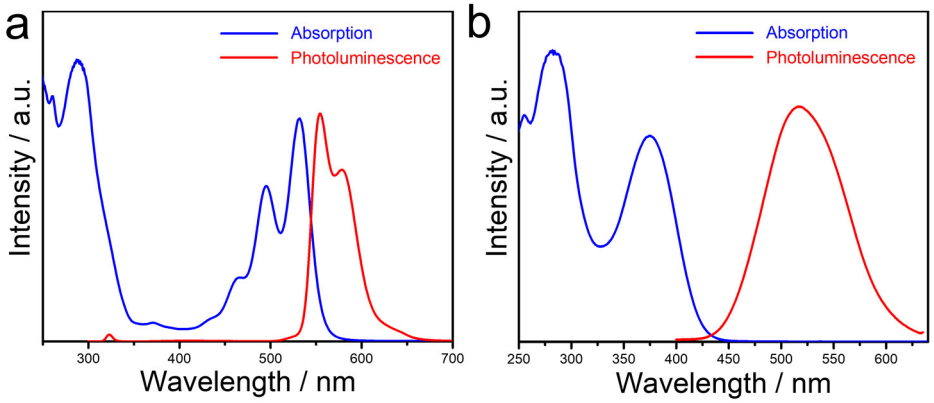

Figure S15. Absorption and photoluminescence spectra of (a) *D*-M_1 and (b) M_2. ($CHCl_3/CH_3CN$ = 1 : 1, *v*/*v*, 0.1 mM). λ_{ex} = 490 nm for *D*-M_1, λ_{ex} = 375 nm for M_2.

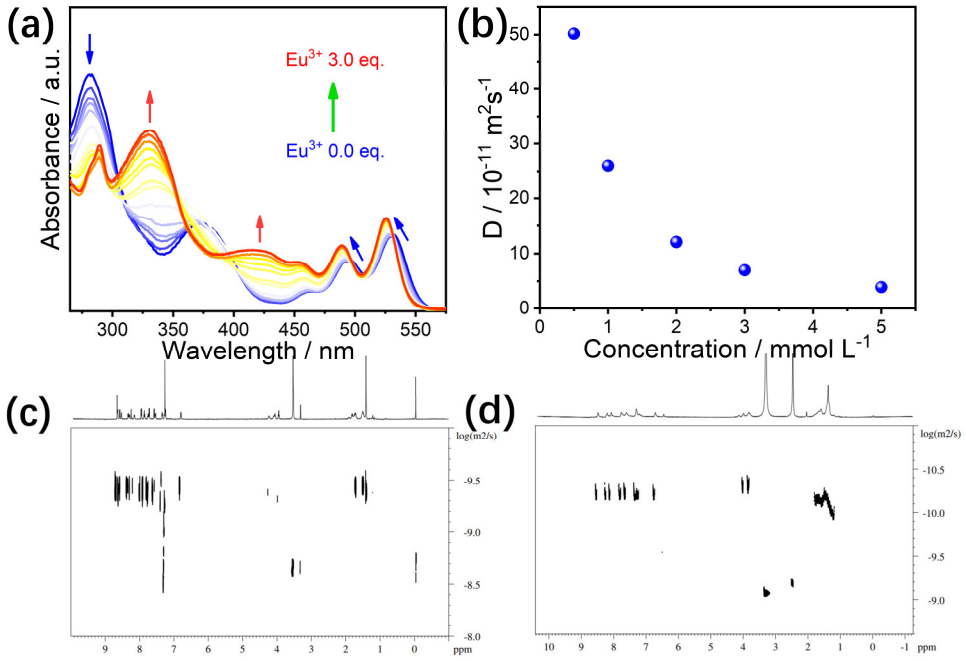

Figure S16. (a) UV–Vis change upon gradual addition of Eu^{3+} into the mixture solution of *D*-M_1 and M_2 (1 : 1 molar ratio, $CHCl_3/CH_3CN$ = 1 : 1, *v*/*v*, 0.1 mM). The bands of 260–300 nm and 330–425 nm are assigned to the π–π* transition of terpyridine, and the band of 430–560 nm is contributed by the 0–1 and 0–0 electronic transitions of PDI. the red-shifted band located at 330 nm is assigned to the metal-ligand charge transfer between terpyridine and Eu^{3+}. (b) DOSY plot (600 MHz, DMSO-d_6, 298 K) of SCPs at concentrations of 0.1, 0.5, 1.0, 3.0, and 5.0 mM. DOSY spectra of SCPs formed from the metal-ligand coordination of *D*-M_1 and M_2 with Eu^{3+} ions at different concentration: (c) 0.1 mM, (d) 5.0 mM. The diffusion coefficients are plotted in a logarithmic scale against the chemical shift.

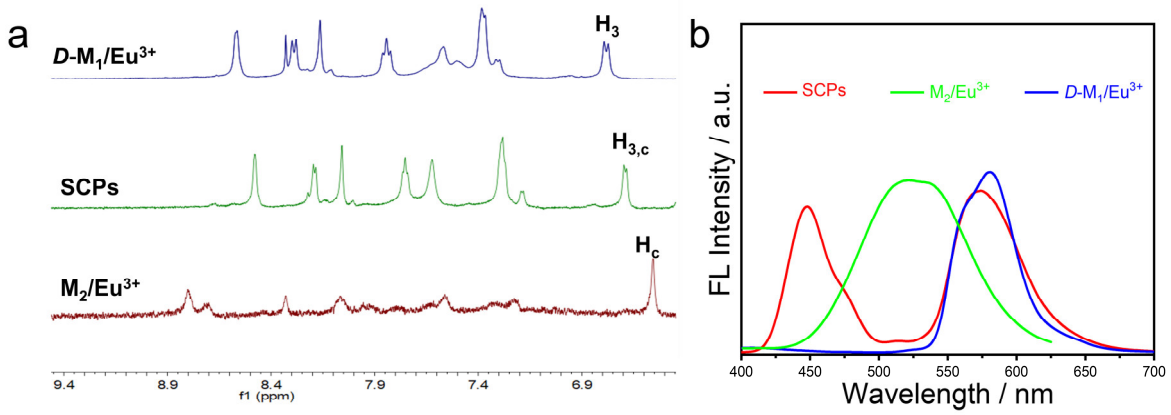

Figure S17. (a) ^{1}H NMR spectra (400 MHz, DMSO-d_6, 1 : 1, *v*/*v*, 298 K, 5 mM) of the complexes of *D*-M$_1$/Eu^{3+} (top), SCPs (middle), and M$_2$/Eu^{3+} (bottom). (b) Fluorescence spectra of SCPs, *D*-M$_1$/Eu^{3+} and M$_2$/Eu^{3+} in toluene. The aromatic resonances of H$_3$ and H$_c$ in SCPs were different from that of *D*-M$_1$/Eu^{3+} (the complex obtained from *D*-M$_1$ and Eu^{3+}) and M$_2$/Eu^{3+} (the complex obtained from M$_2$ and Eu^{3+}), and located between H$_3$ in *D*-M$_1$/Eu^{3+} and H$_c$ in M$_2$/Eu^{3+}. Moreover, fluorescence spectra clearly showed that the complexes of the mono-component *D*-M$_1$/Eu^{3+} and M$_2$/Eu^{3+} existed single emission band centered at 581 nm and 518 nm, respectively, which were different from the dual emission bands of SCPs (545 nm and 575 nm, Figure S17b). If SCPs, *D*-M$_1$/Eu^{3+} and M$_2$/Eu^{3+} coexist in one system, their overlapping spectra will be observed. The results proved that the copolymerization of *D*-M$_1$ and M$_2$ with Eu^{3+} ions definitely dominated the SCPs, instead of the coordination of the mono-component *D*-M$_1$ or M$_2$ with Eu^{3+} ions.

Search for suitable solvents for the further self-assembly of SCPs.

The intermolecular π–π stacking and hydrogen bonds formed by the π-conjugated PDI and amino acids moieties of SCPs are sensitive to solvent polarity. Thus, we first sought to search for suitable solvents for the further self-assembly of SCPs. In a highly polar solvent such as dichloromethane or *N*,*N*-dimethylformamide, SCPs presented a typical non-aggregated state as dissolved, whereas a new red-shifted shoulder band between 550−600 nm appeared in poorly polarizable solvents such as toluene, owing to the π–π stacking of PDI units. Meanwhile, SCPs showed two fluorescence bands at 549 and 575 nm in dichloromethane, which is clay-bank emission color. Upon switching the solvent to toluene, the fluorescence intensity of SCPs decreased markedly and a new band at 448 nm appeared. Such phenomena indicated that solvent polarity possesses a large effect on the aggregation of SCPs. Furthermore, the supramolecular chirality of SCPs was investigated by CD and CPL measurements. As is evident from Fig. S18c, d, the toluene solution of SCPs showed a negative and a positive Cotton effect

in the regions of 470−490 nm and 530−560 nm, respectively, indicating that SCPs could self-assemble in toluene to form regular aggregates. A moderate CPL signal was then detected in toluene with a g_{lum} value of +1.2 × 10^{-3}. Thus, we will focus on the self-assembly behaviors of SCPs in toluene solution in the next studies.

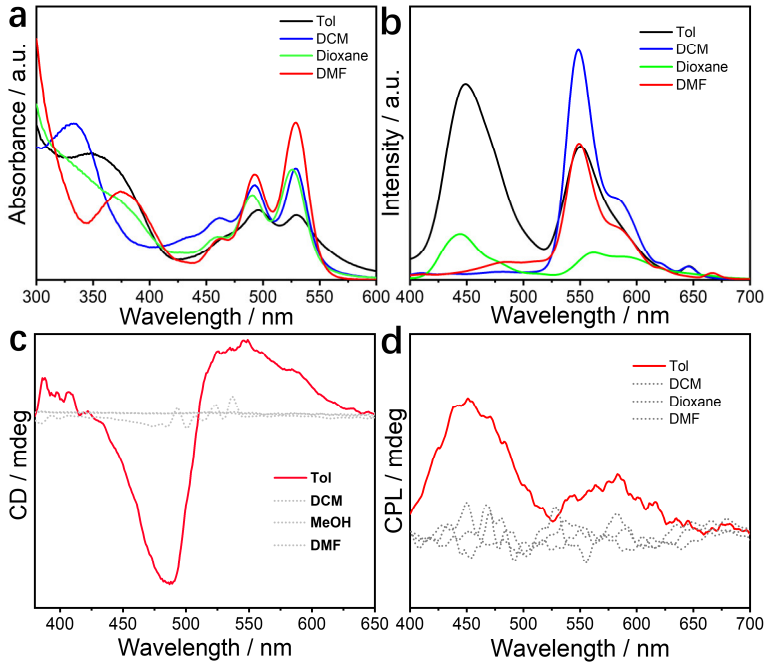

Figure S18. (a) UV–Vis, (b) fluorescence, (c) CD, and (d) CPL spectra of SCPs in different solvents. Concentration: 0.1 mM.

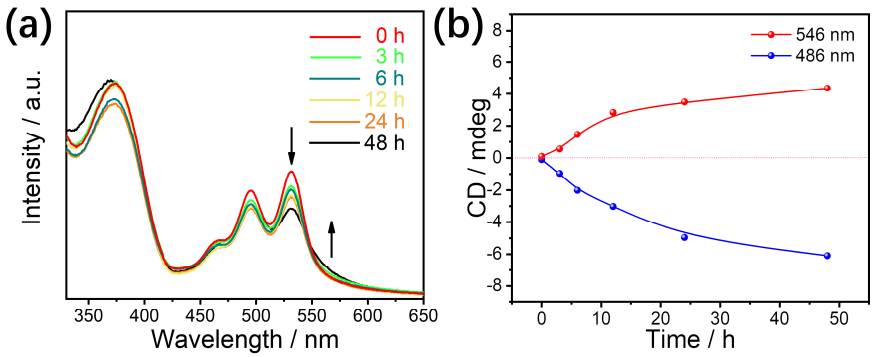

Figure S19. (a) Time-dependent UV–Vis spectra of SCPs in toluene. (b) CD intensity changes at 486 nm and 546 nm versus incubation time. Concentration: 0.4 mM.

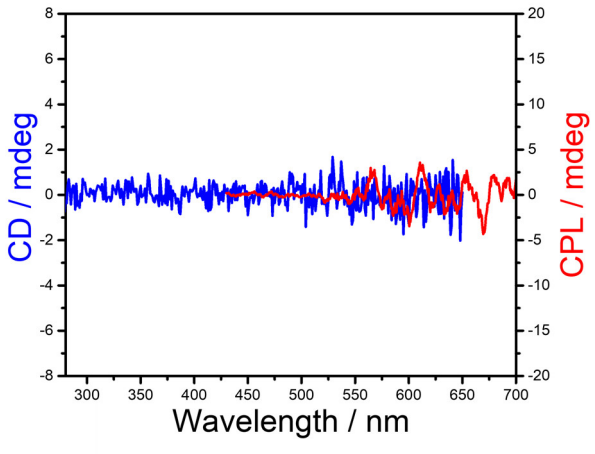

Figure S20. CD (blue line) and CPL (red line) spectra of *D*-M_1/Eu^{3+} in toluene. Concentration: 0.1 mM.

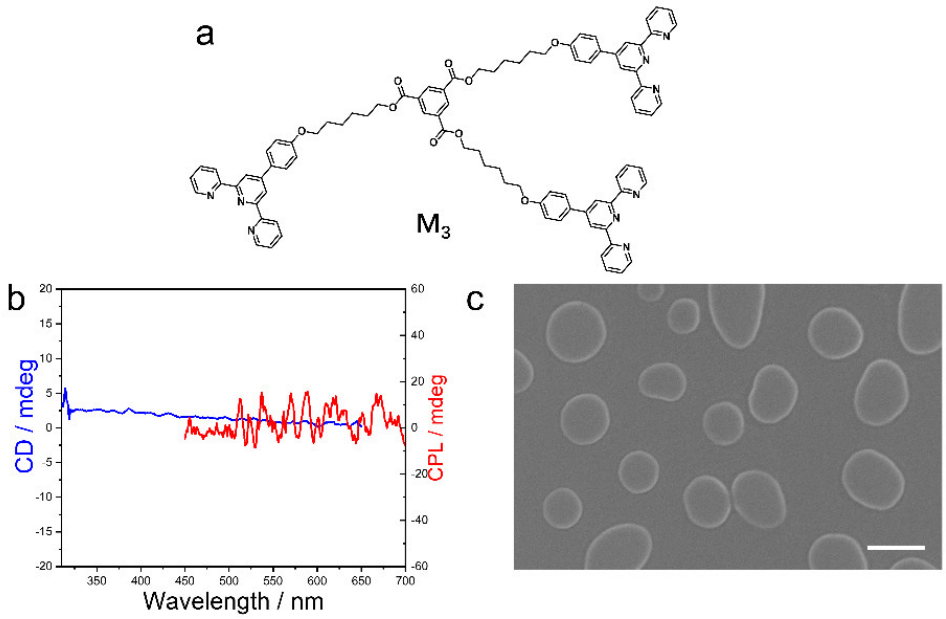

Figure S21. (a) Molecular structure of M_3. (b) CD (blue line) and CPL (red line) spectra and (c) SEM image of complexes constructed by monomers *D*-M_1, M_3 with Eu^{3+}. Scale bar: 500 nm. These control experiments confirmed that the rigid structure of monomer M_2 is beneficial to the chiral amplification of SCPs. Concentration: 0.1 mM.

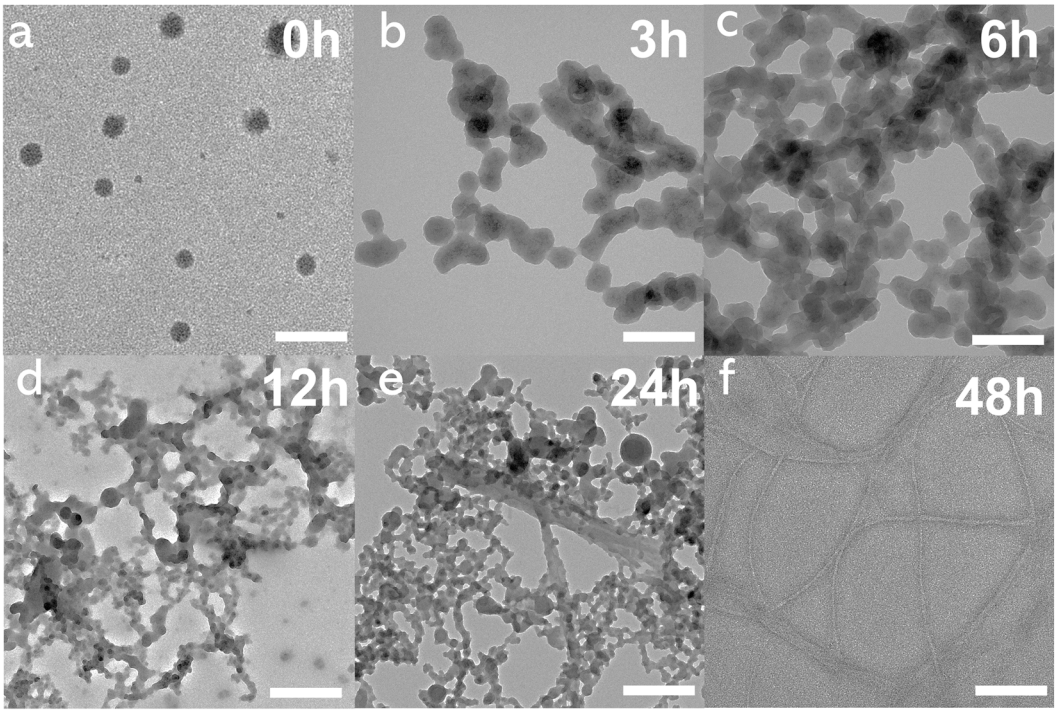

Figure S22. Time-dependent TEM images to visualize the self-assembly process of SCPs: (a) 0 h, (b) 3 h, (c) 6 h, (d) 12 h, (e) 24 h, (f) 48 h. Scale bar: 200 nm. 0.4 mM.

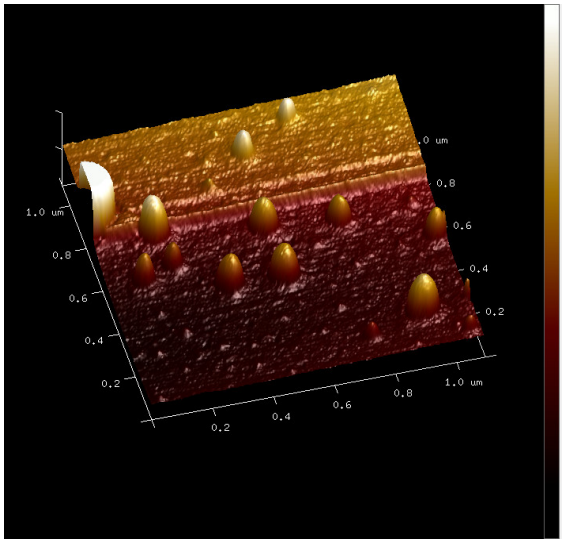

Figure S23. 3D AFM image of SCPs in the initial stage.

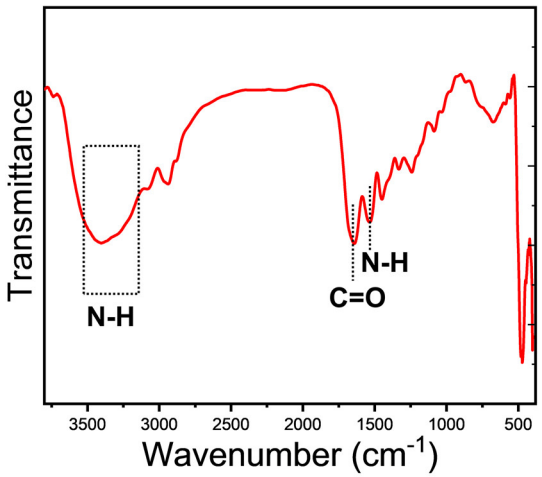

Figure S24. FT-IR spectra of SHNWs. The hydrogen bonds could be verified through FT-IR spectra experiments. The appearance of an N–H stretching vibration band at 3386 cm^{-1}, and the amide I and II bands at 1640 cm^{-1} and 1540 cm^{-1}, indicated that both C=O and N–H in SHNWs were in the hydrogen-bonded form.

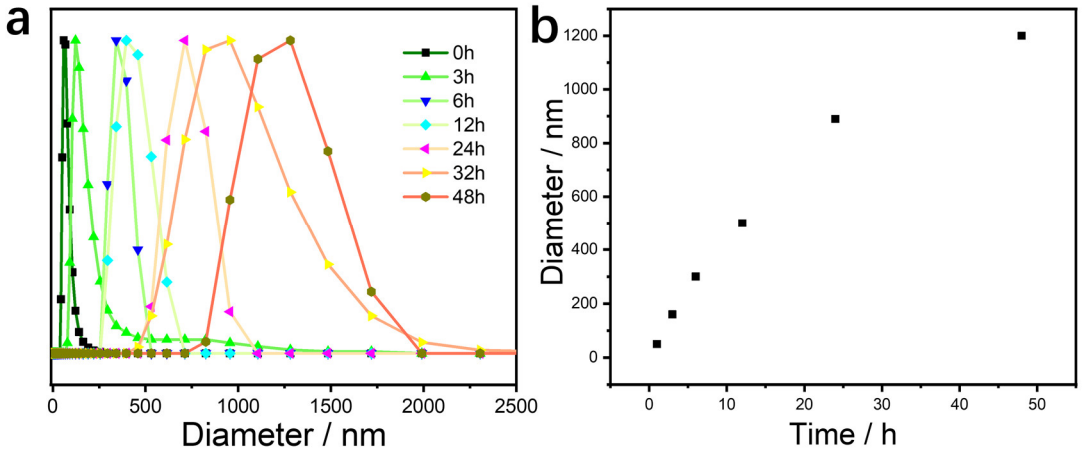

Figure S25. DLS size distribution of SCPs in toluene upon increasing incubation time.

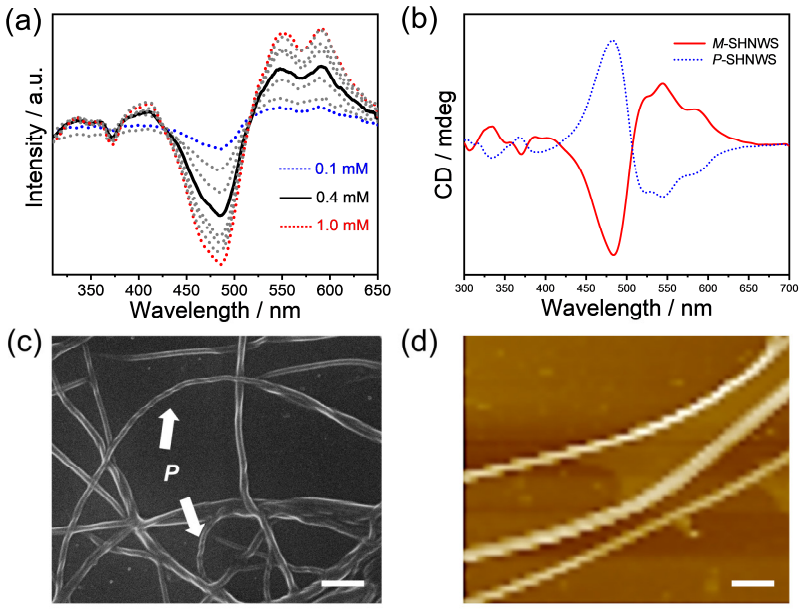

Figure S26. (a) CD spectra of *M*-SHNMs in toluene at different concentrations (0.1–1.0 mM). (b) CD spectra of *M*-SHNWs and *P*-SHNWs in toluene at the concentration of 0.4 mM. (c) SEM and (d) AFM images of *P*-SHNWs in toluene at the concentration of 0.4 mM. Scale bar: 200 nm.

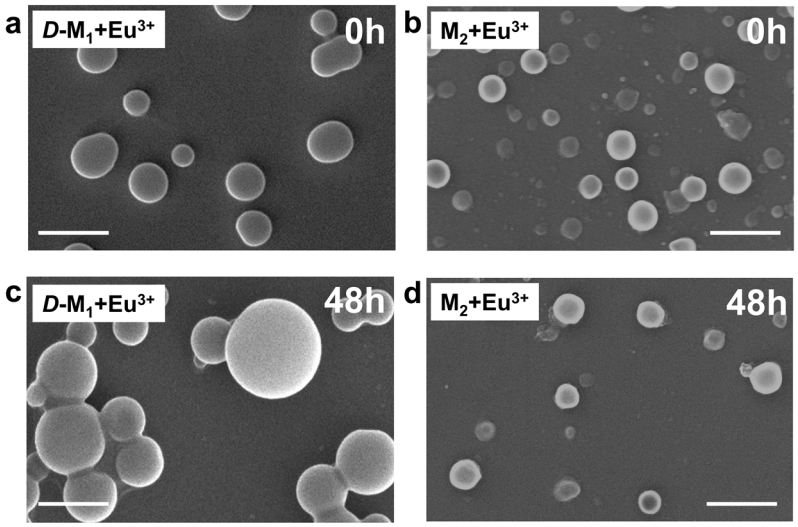

Figure S27. SEM images of the freshly prepared (a) *D*-M_1/Eu^{3+} and (b) M_2/Eu^{3+}, and incubating (c) *D*-M_1/Eu^{3+} and (d) M_2/Eu^{3+} for 48 h. Scale bar: 500 nm. (0.1 mM). As a control experiment, the morphologies of the complexes constructed by individual *D*-M_1 or M_2 with Eu^{3+} ions exhibited large-sized micelles with ~287 nm and 188 nm diameters, respectively. After incubating at the same conditions for 48 h, the morphology of these micelles was no evident change. Thus, the above results indicated that SCPs constructed by the coordination of terpyridine groups from *D*-M_1 and M_2 with Eu^{3+} play a decisive role in the hierarchical self-assembly process.

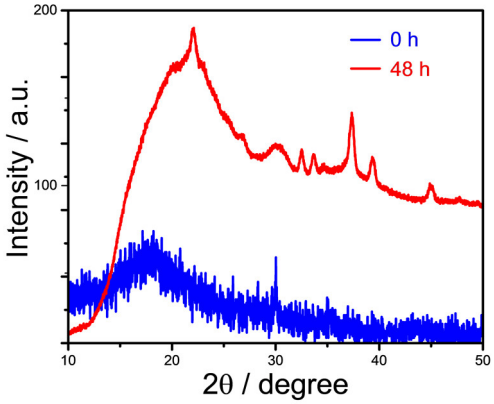

Figure S28. XRD patterns of SCPs incubated at 298 K for 0 h (blue line) and 48 h (red line).

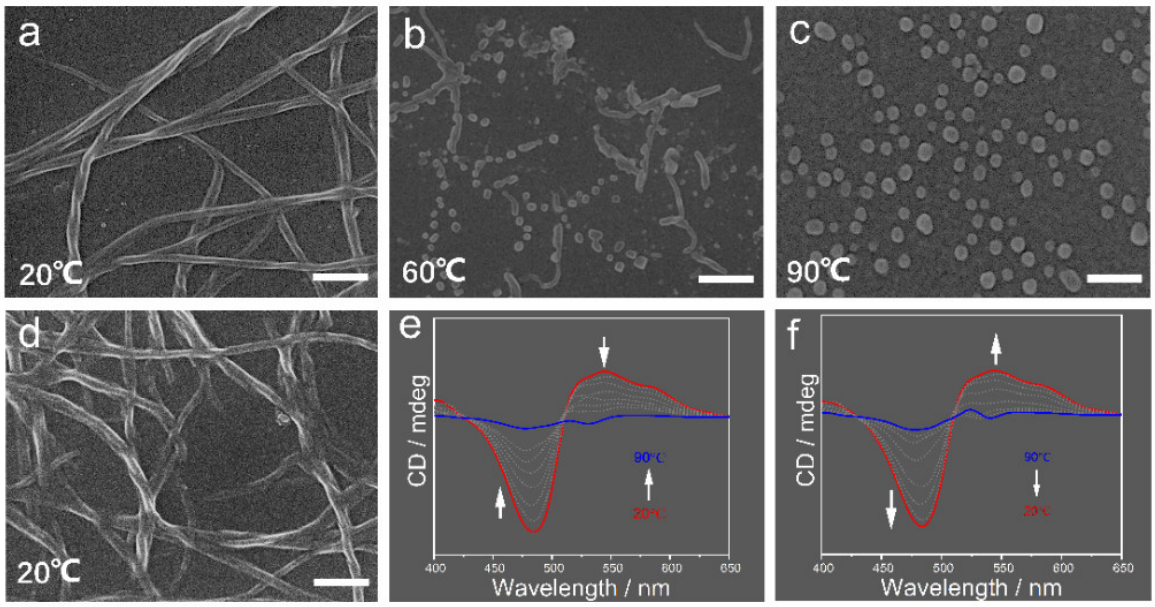

Figure S29. Morphology changes of *M*-SHNWs upon heating from (a) 20 ℃ to (b) 60 ℃ and (c) 90 ℃, then cooling to (d) 20 ℃. Scale bar: 200 nm. (e) and (f) Temperature-dependent CD spectra variations of *M*-SHNWs in toluene (1.0 mM).

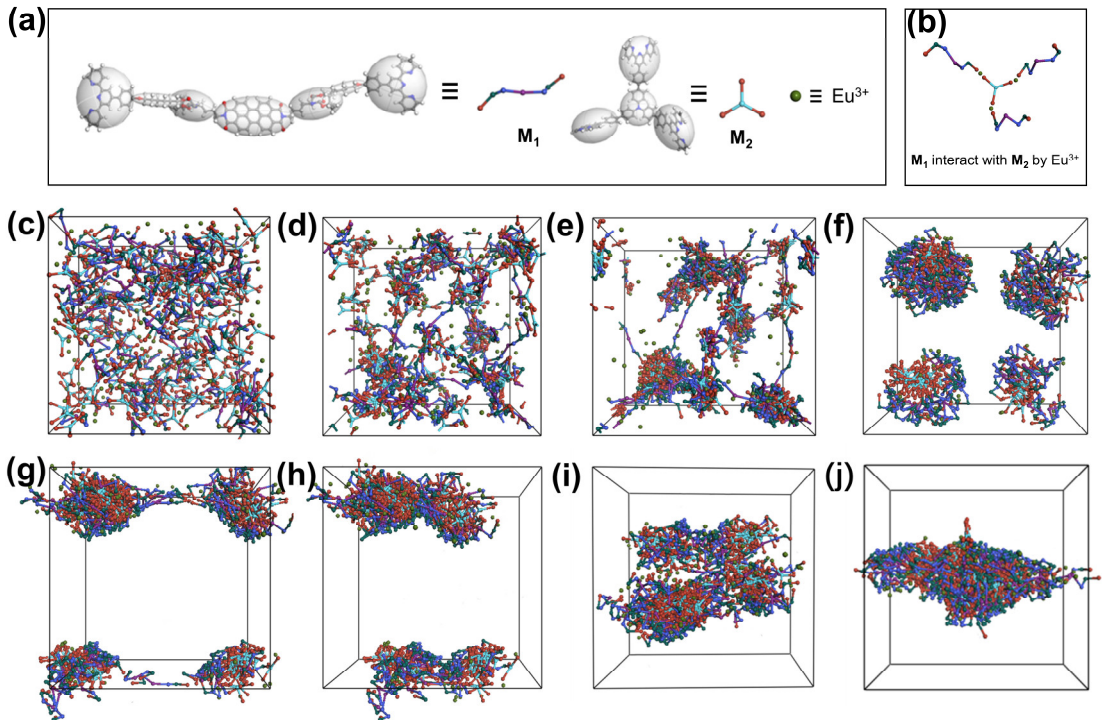

Figure S30. DPD simulations for the hierarchical self-assembly of SCPs. (a) The coarse-grained models of *D*-M_1, M_2 and Eu^{3+}. (b) The model of *D*-M_1 interacts with M_2 by Eu^{3+}. DPD simulations for the self-assembly of SCPs were captured at different time intervals: (c) Initial state, (d) 1.0×10^3 time steps, (e) 5.0×10^3 time steps, (f) 8.0×10^3 time steps, (g) 1.0×10^4 time steps, (h) 3.0×10^4 time steps, (i) 5.0×10^4 time steps, and (j) 8.0×10^4 time steps. Solvent beads are omitted for clarity.

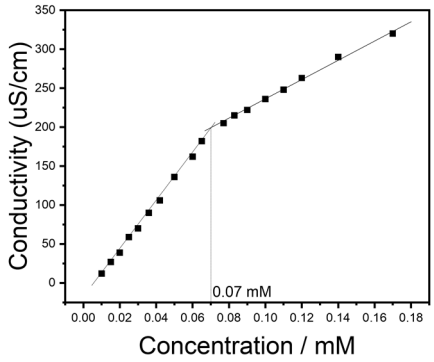

Figure S31. The concentration-dependent conductivity of SCPs.

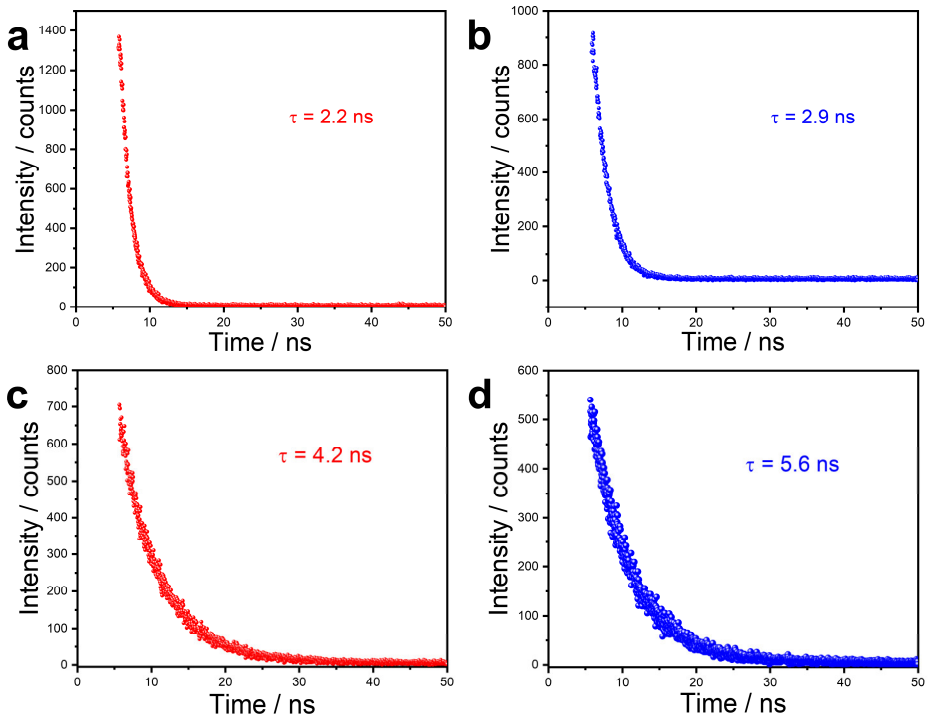

Figure S32. Fluorescence decays of *M*-SHNWs monitored at 454 nm (a) 0.1 M; (b) 1.0 mM and 575 nm (c) 0.1 mM (d) 1.0 mM. (λ_{ex} = 330 nm) at 298K.

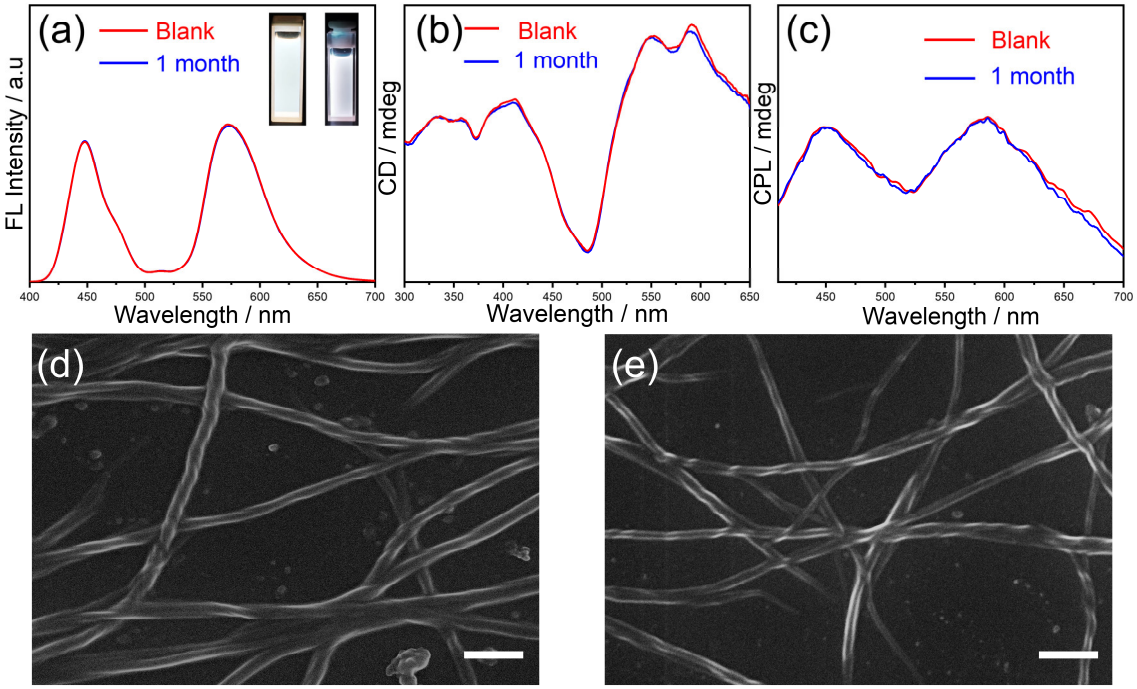

Figure S33. (a) Fluorescence spectra and inset of fluorescence photographs of *M*-SHNWs (left: blank, right: after one month) under 365 nm UV light. (b) CD and (c) CPL spectra of *M*-SHNWs in different time. SEM images of *M*-SHNWs after (d) 48 h and (e) one month.

Comparison experiments

In comparison, for the complexes constructed through the coordination of *D*-M_1 and M_2 with other transition metal ions (Zn^{2+}, Cu^{2+}, Ni^{2+} and Ru^{3+}), the white-light emission color and chiral amplification couldn't be achieved, indicating the complexes of terpyridine-Eu^{3+} assisted the generation of white-light emission. Additionally, no multi-color tunable behaviors were observed for the micelles of mono-component M_2 with Eu^{3+} ions, because of its single emission band feature. For the micelles formed by *D*-M_1 with Eu^{3+} ions, the main emission bands only covered from 525 nm to 650 nm upon varying the concentration, which failed to realized multi-color emission regulation. The above results implied that only the resultant SHNWs from the hierarchical self-assembly of *D*-M_1 and M_2 with Eu^{3+} could lead to white CPL.

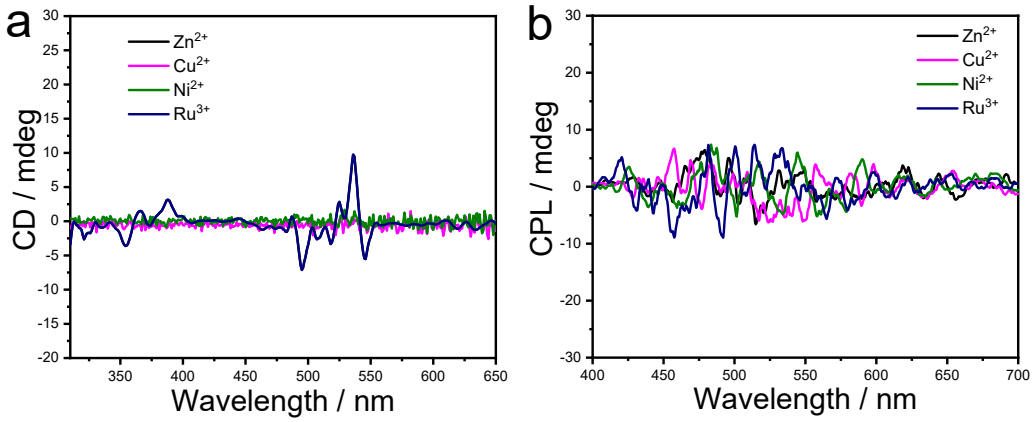

Figure S34. (a) CD and (b) CPL spectra of complexes in toluene obtained from monomers *D*-M_1, M_2 with different metal ions (0.1 mM).

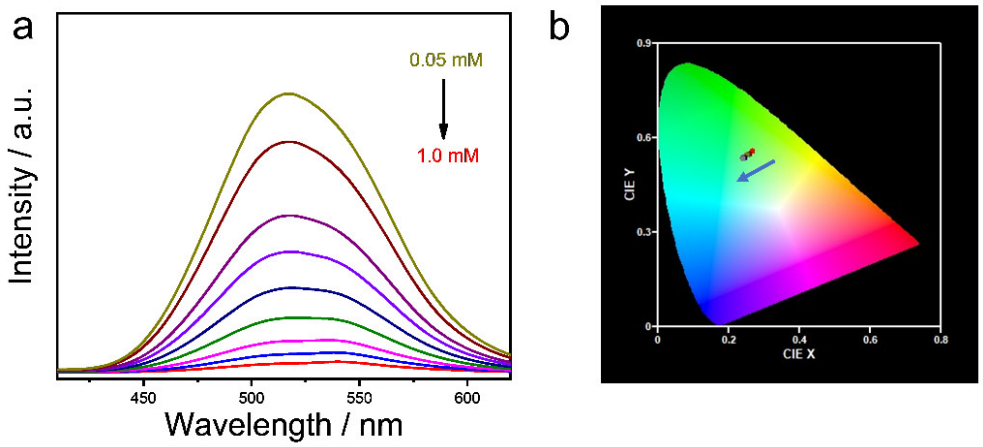

Figure S35. Fluorescence spectra and CIE coordinate changes of M_2/Eu^{3+} in toluene at different concentrations (from 0.05 to 1.0 mM).

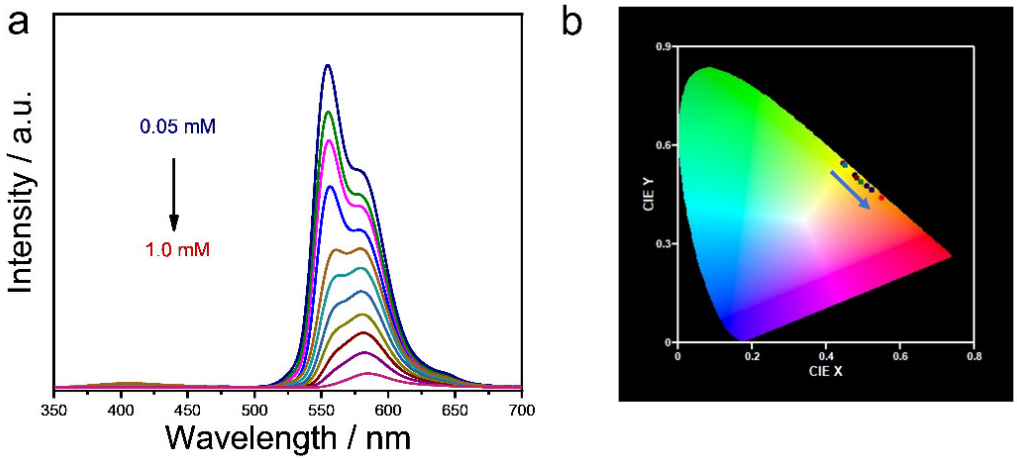

Figure S36. Fluorescence spectra and CIE coordinates changes of *D*-M_1/Eu^{3+} in toluene at different concentrations (from 0.05 to 1.0 mM).

Table S1. Fluorescence quantum yield of *M*-SHNWs at different concentrations.

Concentrations (mM)	0.05	0.1	0.2	0.3	0.4	0.5	0.6	0.7	0.8	0.9	1.0
Φ	0.67	0.61	0.58	0.51	0.47	0.42	0.35	0.29	0.22	0.19	0.14

4. References

(1) (a) Ghosh, A. K.; Hoek, E. M. *J. Membr. Sci*. **2009**, *336*, 140-148; (b) Trivedi, J. S.; Bhalani, D. V.; Bhadu, G. R.; Jewrajka, S. K. *J. Mater. Chem. A*, **2018**, *6*, 20242-20253.

(2) (a) Morgan, P. W.; *Interscience Publishers*, **1965**; (b) Raaijmakers, M. J.; Benes, N. E. *Prog. Polym. Sci*. 2016, 63, 86-142.

(3) Sun, H.; *J. Phys. Chem. B*, **1998**, *102*, 7338-7364.

(4) Qiu, S.; Gao, Z.; Yan, F.; Yuan, H.; Wang, J.; Tian, W. *Chem. Commun*. **2020**, *56*, 383-386.